

The impact of quantum noise on limit cycles and entrainment in an atom-cavity system

Richelle Jade L. Tuquero¹ and Jayson G. Cosme¹

¹National Institute of Physics, University of the Philippines, Diliman, Quezon City 1101, Philippines

(Dated: August 1, 2024)

Quantum noise is inherent in any open quantum system as it affects not only the statistical properties of the initial state but also the time evolution of the system. A transversely pumped atom-cavity setup is a prototypical example of such an open system, wherein limit cycles (LCs) have been observed and identified as continuous time crystals (CTCs). Using truncated Wigner approximation (TWA), we show that the inherent quantum noise pushes the system to exhibit signatures of LCs for interaction strengths lower than the critical value predicted by mean-field theory, suggesting a noise-induced enhancement of temporal ordering. By comparing the oscillation frequencies of the LCs for the one-dimensional (1D) and two-dimensional (2D) regimes, we find that the LC frequencies have larger shot-to-shot fluctuations in 1D than in 2D. We demonstrate that this has an important consequence in the effectiveness of entrainment of LCs for a periodically driven pump intensity or light-matter coupling strength.

I. INTRODUCTION

Typically, noise is expected to inhibit well-defined oscillatory response in complex systems. Nevertheless, it has been suggested that noise could induce order, instead of the expected chaotic behavior [1]. Indeed, phase synchronization in systems with common noise [2] and uncorrelated noise [3] has been observed. Moreover, applied noisy drive has been shown to produce nontrivial ordered phases in interacting quantum systems [4, 5] and, in other cases, can have the opposite effect of destabilizing an existing LC or CTC [6]. In Ref. [7], fluctuations corresponding to the intrinsic quantum property and coupling to an external environment, and their role on the stability of discrete time crystals have been explored. In this work, we focus on the role of inherent quantum noise in the emergence and stability of LCs, particularly in the context of CTCs and their dynamical control [6, 8–11]. These LCs are characterized by oscillating observables at a well-defined frequency even though the underlying equations governing the system's time evolution is manifestly time-independent.

The emergence of LCs in various many-body quantum systems is widely studied, especially in the context of time crystals [6, 12–14]. In particular, for an atom-cavity system [6], artificial noise applied to the light-matter interaction strength is found to destabilize the LC, which then begs the question if the inherent fluctuation associated with the photon dissipation in the cavity [15, 16] could inhibit the appearance of LCs. This is important in understanding the quantum nature of LCs in open systems [17]. Exploring the precise role of quantum noise can be experimentally challenging as the inherent noise cannot be turned off naturally in experiments. However, in a theoretical setting, an approach such as the truncated Wigner approximation (TWA) [18] allows for the possibility of choosing which noise to be included in the theoretical description of a given system. In atom-cavity systems, beyond mean-field approximation of the quantum dynamics using TWA has been shown to capture the correct qualitative behaviour of time crystals observed in experiments [19–21].

In this paper, we investigate the effects of quantum noise on the robustness and dynamics of the LC phase in the 1D and 2D atom-cavity systems. To this end, we employ both mean-

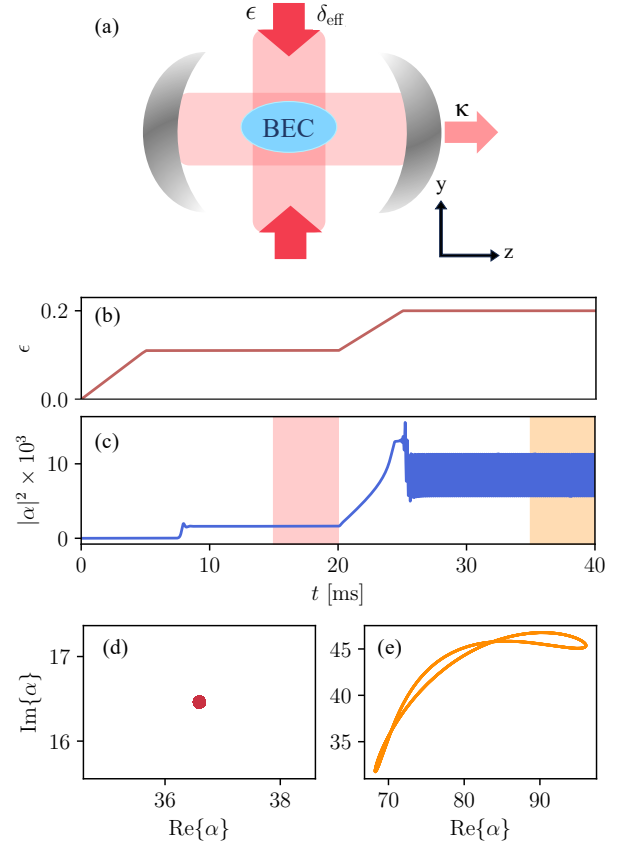


FIG. 1. (a) Schematic diagram of an atom-cavity system with dissipation rate κ and wavelength λ . The laser pump intensity is ϵ with effective detuning δ_{eff} . To exemplify the dynamics of the superradiant and limit cycle phase, we apply a (b) two-ramp pump protocol. (c) Corresponding dynamics of the intracavity photon number. (d), (e) Long-time trajectories in a complex plane spanned by $\text{Re}\{\alpha\}$ and $\text{Im}\{\alpha\}$ for the (d) SR phase and (e) LC phase.

field simulations and TWA, wherein we sample the quantum noise of the initial state and the stochastic noise in time. In doing so, we can compare the dynamics for cases with and without quantum noise. This allows us to infer the effects of quantum noise to the emergence of LCs. Moreover, we investigate the entrainment of LCs [11] in both 1D and 2D by

periodically driving the pump intensity. Consequently, we are able to observe a hallmark of entrainment, which is frequency locking, and we determine which of the atom-cavity systems will exhibit a more robust entrainment.

This paper is structured as follows. We first discuss the atom-cavity system in Sec. II. Next, we present the mean-field diagrams for the 1D model in Sec. III. We also show the spectrogram for different values of the pump intensity. In Sec. IV A, we analyze the average response frequencies together with the corresponding standard deviation to infer the qualitative and quantitative effects of quantum noise. We compare the entrainment of LCs for the 1D and 2D atom-cavity systems in Sec. IV B. Lastly, we conclude the paper in Sec. V.

II. ATOM-CAVITY MODEL

We focus on a model for an atom-cavity system of ^{87}Rb atoms forming a Bose-Einstein condensate (BEC) with particle number $N_a = 6.5 \times 10^4$ trapped inside a Fabry-Pérot resonator as shown in Fig. 1(a). A pump beam with intensity $\varepsilon = \epsilon E_{\text{rec}}$, where $E_{\text{rec}} = \hbar\omega_{\text{rec}}$ is the recoil energy, is applied in the direction perpendicular to the cavity axis. The pump has a wavelength $\lambda_p = 792.55$ nm and the recoil frequency is $\omega_{\text{rec}} = 2\pi^2\hbar/m\lambda_p$, where m is the mass of a ^{87}Rb atom. Photons leaking out of the cavity is characterised by the cavity photon decay rate $\kappa = 2\pi \times 3.6$ kHz. We use realistic parameters based on experimental realizations in the good cavity regime $\kappa \sim \omega_{\text{rec}}$ [6, 9–11, 22].

The Hamiltonian for the atom-cavity system consists of cavity, atom, and atom-cavity interaction terms

$$\hat{H} = \hat{H}_C + \hat{H}_A + \hat{H}_{AC}. \quad (1)$$

Here, we neglect the contact interaction between the atoms, which corresponds to a mean-field breaking term in this model [20]. The Hamiltonian for the cavity with a mode function $\cos(kz)$ is given by

$$\hat{H}_C = -\hbar\delta_C\hat{\alpha}^\dagger\hat{\alpha}, \quad (2)$$

where δ_C is the pump-cavity detuning and $\hat{\alpha}^\dagger$ ($\hat{\alpha}$) is the creation (annihilation) operator for the cavity photon. Note that $\delta_C = \delta_{\text{eff}} + N_a U_0/2$, where U_0 is the lattice depth induced by a photon in the cavity. The Hamiltonian for the atoms is

$$\hat{H}_A = \int \hat{\Psi}^\dagger(y, z) \left[-\frac{\hbar^2}{2m}\nabla^2 + \varepsilon \cos^2(ky) \right] \hat{\Psi}(y, z) dy dz \quad (3)$$

where $\hat{\Psi}(y, z)$ is the bosonic field operator associated with the BEC. Lastly, we consider the atom-cavity interaction

$$\hat{H}_{AC} = \int \hat{\Psi}^\dagger(y, z) \hbar U_0 [\cos^2(kz)\hat{\alpha}^\dagger\hat{\alpha} + \sqrt{\frac{\varepsilon}{\hbar|U_0|}} \cos(kz) \cos(ky) (\hat{\alpha}^\dagger + \hat{\alpha})] \hat{\Psi}(y, z) dy dz. \quad (4)$$

In the 1D limit, the dynamics along the pump direction is frozen $\hat{\Psi}(y, z) \rightarrow \hat{\Psi}(z)$, such that Eq. 3 reduces to just the

kinetic energy along the cavity direction. Moreover, the atom-cavity interaction Eq. 4 simplifies to only contain z -dependent terms, which can be obtained by taking $\cos(ky) \rightarrow 1$. The dynamics of the system is given by the Heisenberg-Langevin equations

$$\frac{\partial}{\partial t} \hat{\Psi} = \frac{i}{\hbar} [\hat{H}, \hat{\Psi}] \quad (5)$$

$$\frac{\partial}{\partial t} \hat{\alpha} = \frac{i}{\hbar} [\hat{H}, \hat{\alpha}] - \kappa\hat{\alpha} + \xi, \quad (6)$$

where ξ is the stochastic noise due to the cavity dissipation with $\langle \xi^*(t)\xi(t') \rangle = \kappa\delta(t-t')$ [15, 16].

In our numerical simulations, we represent the quantum operators as c -numbers using TWA. This enables us to approximate the dynamics using an ensemble of stochastic trajectories. The TWA includes the leading order quantum corrections to the mean-field theory, which is valid for $N_a \rightarrow \infty$ [18, 23, 24]. In open quantum systems, perturbations due to quantum noise in the initial states and stochastic noise ξ associated with the photon loss are present. In theory, we can choose which source of quantum noise we include in our TWA simulations. To numerically solve the relevant stochastic differential equations, we utilize the predictor-corrector method, otherwise known as Heun's method. We consider a time step of 10^{-8} s and record the values every 20 steps. For 1D simulations, we use a real-space basis for $\hat{\Psi}(z)$ [20], while for 2D simulations, we employ a momentum-space basis for $\hat{\Psi}(y, z)$ [11, 21].

III. MEAN-FIELD RESULTS

In this section, we first focus on mean-field simulations to serve as a benchmark for TWA simulations, which will be shown in the next section.

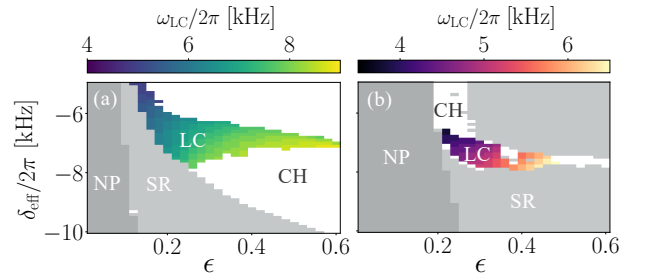


FIG. 2. Phase diagram of a one-dimensional atom-cavity system when (a) $U_0 = 2\pi \times 0.7$ Hz for the blue-detuned case, and (b) $U_0 = -2\pi \times 0.34$ Hz for the red-detuned case. We show the Normal phase (NP), Superradiant (SR), limit cycle (LC), and Chaos (CH). The LC phase includes the frequencies as given by the color bar on top.

To introduce the phases found in this configuration of an atom-cavity system, we implement the two-ramp pump protocol shown in Fig. 1(b). In Fig. 1(c), we show the dynamics of the intracavity photon number, $|\alpha|^2$, used to distinguish between different phases in the system. The normal phase (NP)

is identified by a zero intracavity photon number. By increasing the pump intensity, it will transition to the superradiant phase (SR) when $\varepsilon \geq \varepsilon_{\text{SR}}$, where ε_{SR} is the critical value for the NP-SR transition. The SR phase is characterized by a non-zero constant intracavity photon number [15, 25–27] as highlighted in Fig. 1(c). Hence, its long-time trajectory as shown in Fig. 1(d) is a steady state in the phase space spanned by the real and imaginary parts of the cavity mode α . Increasing the pump intensity further leads to a transition into the LC phase. This dynamical phase is characterized by an oscillating $|\alpha|^2$ at a well-defined limit cycle frequency ω_{LC} as shown in Fig. 1(c). Because it oscillates at a certain frequency, the long-time trajectory in phase space forms a closed loop as presented in Fig. 1(e).

In Fig. 2, we present the phase diagram in the $\delta_{\text{eff}}-\varepsilon$ space for a 1D system. We note that the existence of LCs in the 1D regime for blue and red atom-pump detunings was first predicted in Refs. [8] and [28], respectively. To construct Fig. 2, we linearly increase the pump intensity until ε for $t \in [15, 20]$ ms. Then, we fix ε to a constant value for 15 ms. We consider the time frame of the last 5 ms to obtain the long-time average, maximum value, and the standard deviation of the rescaled peak heights of the cavity occupation. In classifying the dynamics, we apply the following threshold values. A cavity occupation dynamics is classified to be that of a LC

if the standard deviations is lower than 0.025, and the difference between the maximum and average $|\alpha|^2$ is greater than or equal to 10% of the average. The SR phase, on the other hand, is identified by having a standard deviation less than 10% of the average cavity occupation. A response with an average photon occupation less than or equal to 10^{-3} is considered as a NP. Lastly, dynamics with standard deviation greater than or equal to 0.025 is determined as a chaotic response (CH). We obtain the LC frequency ω_{LC} from the dominant frequency in the power spectrum dynamics of the intracavity photon number $|\alpha|^2$ for the same time window. Then, ω_{LC} is obtained as the frequency with the highest peak in the power spectrum. In Fig. 2, both the blue-detuned and red-detuned cases have LCs.

In Fig. 3, we further investigate the dynamics of $|\alpha|^2$ by including a gallery of spectrograms for different $\varepsilon/\varepsilon_{\text{LC,MF}}$, where $\varepsilon_{\text{LC,MF}}$ is the intensity required to transition from SR to LC according to MF theory. This allows us to take note of how the dynamics change for different intensities in the absence of stochastic noise. Accordingly, we expect that the system is in the SR phase when $\varepsilon/\varepsilon_{\text{LC,MF}} < 1.0$, and it is in the LC phase when $\varepsilon/\varepsilon_{\text{LC,MF}} \geq 1.0$. For the pump protocol, we linearly increase the pump intensity until the desired ε for 5 ms, then kept it constant for 395 ms. Afterwards, we obtain the spectrogram of $|\alpha|^2$ using a moving time window of ≈ 3.3 ms. The intensity in units of dB corresponds to $10 \log_{10}(P)$ where P is the power spectral density. Hence, the dominant oscillation frequencies of $|\alpha|^2$ are characterized by positive intensity shown as brighter shades in the color bars. Thus, a dominant frequency seen as streak of positive intensity at a constant ω signifies the appearance of a LC. On the other hand, the SR phase is identified by the lack of nonzero frequency peak in the long-time limit due to the absence of photon oscillations.

We find that in 1D, as depicted in Fig. 3(a), transient oscillations appear but they eventually vanish for long times as ε approaches $\varepsilon_{\text{LC,MF}}$. We note for the discussions in the next section that the transient oscillations in Fig. 3 persist for $t < 100$ ms. To inspect these dynamics, we show in Fig. 3(c-f), the adjusted intracavity dynamics $|\alpha|_{\text{ctr}}^2 = |\alpha|^2 - |\alpha|_{\text{mean}}^2$ where $|\alpha|_{\text{mean}}^2$ is the mean value of $|\alpha|^2$ for $t \in [0.1, 0.4]$ s, and its corresponding spectrogram for $\varepsilon/\varepsilon_{\text{LC,MF}} < 1.0$. We find that the amplitude of the $|\alpha|_{\text{ctr}}^2$ oscillation decreases and eventually vanishes. This is also reflected in the features of the spectro-

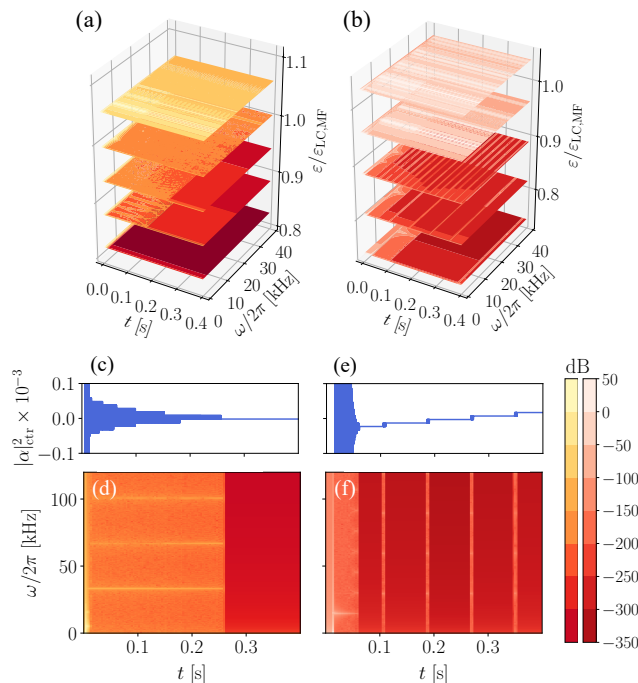


FIG. 3. Gallery of spectrograms for (a) 1D and (b) 2D atom-cavity systems. Each slice corresponds to a pump intensity rescaled by the pump intensity needed to enter the LC phase according to mean-field theory, $\varepsilon/\varepsilon_{\text{LC,MF}}$. The effective detuning for 1D and 2D is $\delta_{\text{eff}} = -2\pi \times 7$ kHz and $\delta_{\text{eff}} = -2\pi \times 4.7$ kHz, respectively. Intracavity photon dynamics and spectrogram for (c-d) 1D with $\varepsilon/\varepsilon_{\text{LC,MF}} \approx 0.94$, and (e-f) 2D with $\varepsilon/\varepsilon_{\text{LC,MF}} \approx 0.81$.

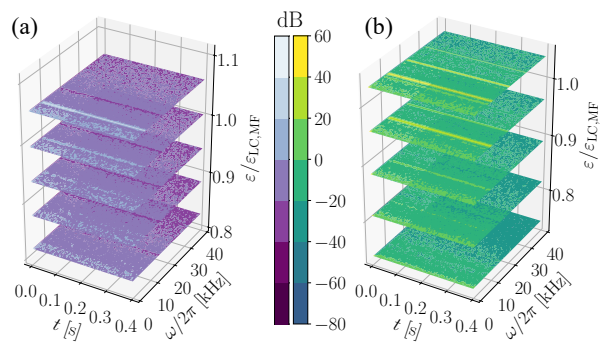


FIG. 4. Spectrograms for (a) 1D and (b) 2D with the same set of parameters as in Fig. 3 but including stochastic noise in the time evolution.

gram in Fig. 3(d). It is also striking that a consistent dominant frequency is present, and that it is larger than the expected ω_{LC} . On the other hand, the 2D system shows a different trend in Fig. 3(b). While we find that the transient oscillations vanish after some time similar to the 1D case, we find that the photon dynamics approach what appears to be plateaus that increase in value as portrayed in Fig. 3(e). Moreover, between these plateaus, we observe short-lived small amplitude oscillations that become more frequent the closer ε is to $\varepsilon_{LC, MF}$. The sharp increase in the photon number appears as streaks at constant times in the spectrogram in Figs. 3(b) and 3(f).

Overall, the mean-field limit provides us with a baseline of the expected behavior of the system. To summarize, we found that transient oscillations are present in the absence of stochastic noise. Hence, one may mistakenly identify these transient oscillatory response as LC if the simulation time is not sufficiently long. We will thus classify such a behaviour with an oscillatory response faster than the expected LC frequency as a SR phase.

IV. TWA SIMULATIONS

A. Noise and limit cycles

In the previous section, we discussed the mean-field dynamics of $|\alpha|^2$ for different pump intensities. Next, we explore the effects of quantum noise in the initial state and stochastic noise associated with the cavity dissipation. We will assume that the stochastic noise in time can be freely switched off within TWA as done in the supplementary materials of Ref. [6]. By comparing the results with and without stochastic noise, we can pinpoint the fundamental effect of stochastic noise.

In Fig. 4, we present the results for the same pump protocol used in Fig. 3 albeit now in the presence of stochastic noise. Note that we use exactly the same initial state for a fair comparison. As expected when temporal noise is included in the dynamics, we find that stochastic noise broadens the power spectrum, which results to a decrease in the intensities of the dominant frequencies. Interestingly, the transient high-frequency oscillations in the SR phase seen in Fig. 3 have vanished in the presence of stochastic noise. This means that the inherent quantum noise due to dissipation overwhelms the transient oscillations making them unlikely to be observed in actual experiments. Moreover, it also pushes the system to oscillate at a well-defined frequency such that $\omega_{\text{peak}} \sim \omega_{LC, MF}$ as seen from the bright streaks close to the expected LC frequency in Fig. 4. This will become more obvious when we discuss Fig. 5 later. The spectrograms for the SR phases close to the SR-LC transition point already show signs of a LC by having a faint bright streak at the expected LC frequency in Fig. 4(b), for example. In the remainder of this section, we will further explore this apparent noise-induced enhancement of the LC phase.

To further investigate the noise-induced temporal ordering, we now use 100 trajectories in our TWA simulations for varying pump intensities as depicted in Figs. 5 and 6 for the

1D and 2D systems, respectively. For the pump protocol, we linearly increased the intensity for 5 ms and then kept it constant for 15 ms. We then analyze the Fourier transform of the intracavity photon number for $t \in [15, 20]$ ms, $F\{|\alpha|^2(t)\} = |\tilde{\alpha}|^2(\omega)$. The dominant frequency ω_{peak} is determined as the frequency corresponding to the maximum value of the normalized Fourier spectrum given by the crystalline fraction defined as $\Xi = \max\{|\tilde{\alpha}|^2(\omega) / \sum_{\omega} |\tilde{\alpha}|^2(\omega)\}$ [29].

In Figs. 5 and 6, we present two sets of results depending on which type of quantum noise is included in the TWA. In both cases, quantum noise in the initial state is included assuming a coherent state for the BEC and a vacuum state for the cavity mode. However, in one case, the stochastic noise is absent meaning the dynamics is fully deterministic, while in the other, it is present resulting to a stochastic dynamics of the system. Furthermore, Fig. 5 depicts the results for the 1D case while Fig. 6 corresponds to the 2D case. In Figs. 5(a) and 6(a), the average values of ω_{peak} for 100 trajectories are indicated as circles and diamonds for those with and without stochastic noise, respectively. The error bars denote the standard deviation for the recorded peak frequencies. In Figs. 5(b)-(g) and 6(b)-(g), we present the histograms of the crystalline fraction and peak frequency for exemplary choices of the pump intensity. Here, the intensity of the color bar represents the number of trajectories following the binning procedure for the histograms.

The SR phase manifests as a zero-frequency oscillation in MF as shown in Fig. 5(b), and low-frequency oscillation due to stochastic noise in Fig. 5(e). Trajectories with significantly high frequency without stochastic noise are attributed to SR phase instead of the LC phase as discussed in Sec. III. These low amplitude high-frequency oscillations emerges the closer the pump intensity is to $\varepsilon_{LC, MF}$. In some trajectories, these high frequencies have a well-defined oscillation as noted by a high value of Ξ in Fig. 6(b) and 6(c). We emphasize that these fast oscillations are transient as discussed in the previous section, which means that all trajectories in Fig. 6(b), for example, correspond to a SR phase. Interestingly, Figs. 5(c), 5(f), 6(c), and 6(f) exhibit trajectories with $\omega_{\text{peak}} \sim \omega_{LC, MF}$ even though $\varepsilon < \varepsilon_{LC, MF}$. More importantly, comparing Figs. 5(c) and 5(f), we find that the presence of stochastic noise in time has eliminated the presence of trajectories in the SR phase oscillating at high frequencies. This phenomenon is even more pronounced in 2D as seen in Figs. 6(c) and 6(f). Hence, the suppression of the high-frequency oscillations in the SR phase by stochastic noise reveals an early signature of the onset of LCs. This noise-induced enhancement of LC is emphasized in Fig. 6(f), in which most trajectories possess $\omega_{\text{peak}} \sim \omega_{LC, MF}$. Nevertheless, we point out that not all trajectories can be considered as LC due to some of them having a relatively low Ξ . Furthermore, the presence of noise in the initial state leads to a shift of the phase diagram because of the slight variations of $N_a U_0$ for constant U_0 . Thus, trajectories would either be an SR or LC near the SR-LC transition since the quantum fluctuations in the initial state effectively changes the δ_{eff} .

To investigate the shot-to-shot fluctuations found deep in

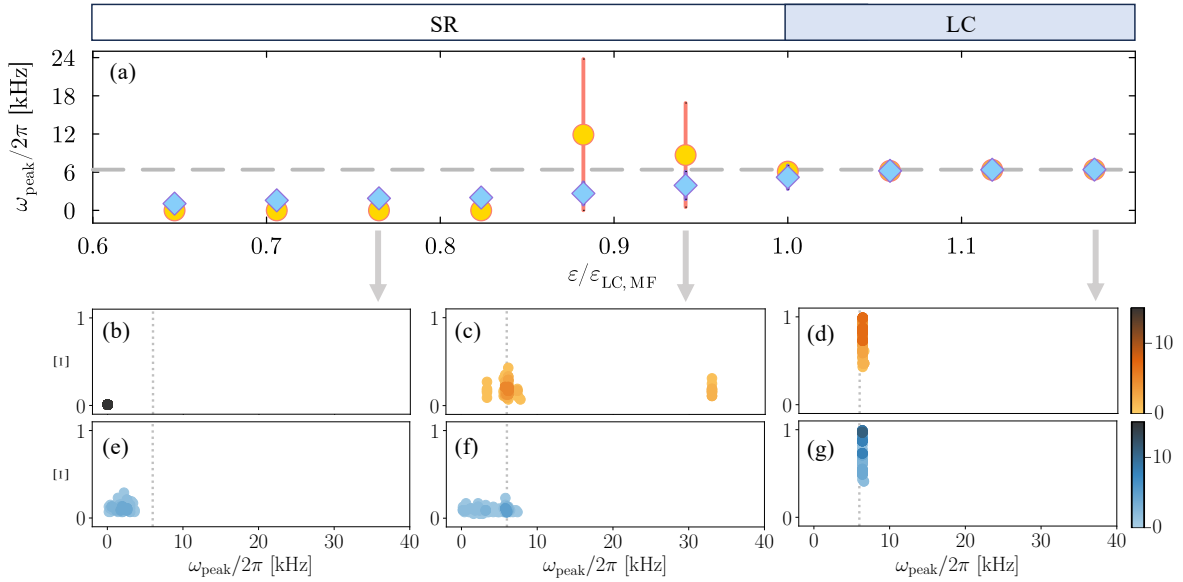


FIG. 5. (a) The mean frequencies with the standard deviation indicated by the error bars for with (diamond) and without (circle) temporal noise for a one-dimensional atom-cavity system when $\delta_{\text{eff}} = -2\pi \times 7$ kHz. The shot-to-shot frequency with the relative crystallization fraction for (b-d) with and (e-g) without noise. The horizontal dashed line in (a) and the vertical dotted lines in (b)-(h) correspond to the mean-field limit cycle frequency, $\omega_{\text{LC}} = 2\pi \times 6.0$ kHz, for the closest limit cycle phase.

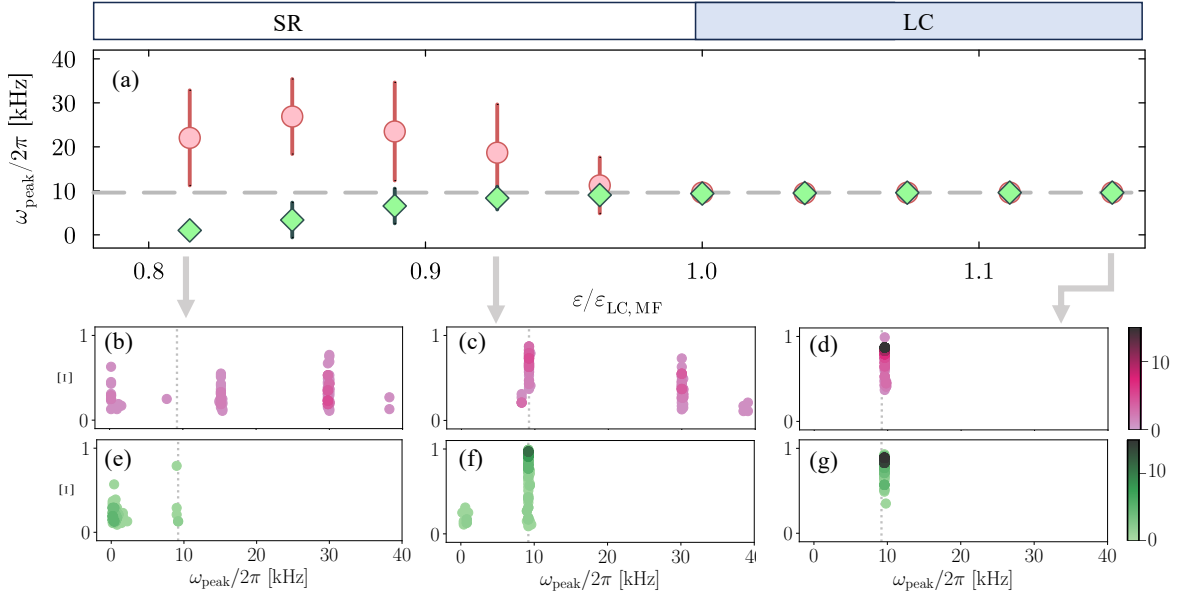


FIG. 6. (a) Similar to Fig. 5 but for a 2D atom cavity system with $\delta_{\text{eff}} = -2\pi \times 4.7$ kHz, and $\omega_{\text{LC}} = 2\pi \times 9.2$ kHz.

the LC regime, we employ TWA for 500 trajectories as shown in Fig. 7. We use the same pump protocol as in the mean-field simulations and kept it constant for 20 ms and 35 ms for 1D and 2D, respectively. We calculate the Fourier transform of the cavity occupation dynamics for each trajectory over the last 5 ms, which means that our Fourier transform can only detect frequency changes larger than 200 Hz. This is important to note when we consider multiple trajectories within TWA as they could in principle have different ω_{LC} . From the Fourier spectrum, we record its real and imaginary

parts at the LC frequency predicted by MF, $N_P(\omega_{\text{LC, MF}})$, for fixed δ_{eff} and ϵ . Furthermore, we rescale the spectrum by the maximum value recorded for all trajectories. Notice that some of the trajectories do not have the same LC frequency as the mean-field prediction, which is evident from the points scattered near the origin of Figs. 7(a) and 7(b). Specifically, we note that some of the trajectories have frequency around $\omega_{\text{peak}} = \omega_{\text{LC, MF}} \pm 2\pi \times 200$ Hz. This can be explained by the smooth variation of the LC frequency in the mean-field phase diagram. Quantum fluctuations in the initial state

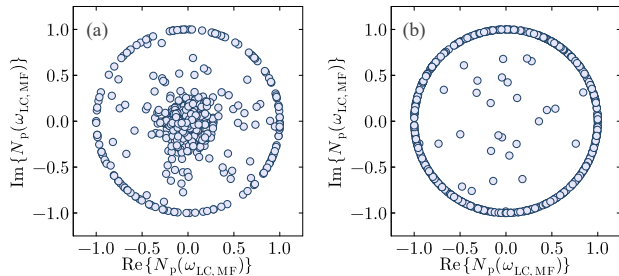


FIG. 7. Distribution of the time phase in the limit cycle phase for 500 trajectories within TWA for the blue-detuned (a) 1D and (b) 2D atom-cavity system. We use (a) $\varepsilon/\varepsilon_{\text{LC,MF}} \approx 1.67$, $\omega_{\text{LC,MF}} = 2\pi \times 8$ kHz, and $\delta_{\text{eff}} = -2\pi \times 7$ kHz and (b) $\varepsilon/\varepsilon_{\text{LC,MF}} \approx 1.59$, $\omega_{\text{LC,MF}} = 2\pi \times 10.6$ kHz, and $\delta_{\text{eff}} = -2\pi \times 7.4$ kHz.

lead to shot-to-shot variations of the total particle number N_a , which means that TWA can be considered as a sampling of MF results from slightly different choices of δ_{eff} in the mean-field phase diagram. This then leads to different LC frequency for each trajectory, the variation of which depends on how fast the LC frequency changes as a function of δ_{eff} . In comparison to Fig. 7(a), we find that there are less fluctuations of the LC frequency in the 2D system as shown in Fig. 7(b), wherein most trajectories are found along the unit circle.

B. Entrainment

We now investigate the consequence of fluctuating LC frequency on the phenomenon of entrainment when the pump intensity is periodically modulated [10, 11]. Entrainment, otherwise known as injection locking in optics, is observed by periodically driving a system with a limit cycle state [30]. This results to the “locking” of the limit cycle frequency by driving the system to a ratio of ω_{LC} [31, 32]. In the atom-cavity system, this was proposed to create a more robust time crystal or limit cycle phase [9] and was later reported experimentally [11]. In both of these papers, they focused on subharmonic injection locking, wherein the pump intensity is periodically driven at a frequency $\omega_{\text{dr}} = 2\omega_{\text{LC}}$.

In the following, we first choose a set of parameters deep in the LC regime with frequency $\omega_{\text{LC,MF}}$. Then, we periodically modulate the pump intensity once we have a stable LC by driving it at twice the LC frequency $\varepsilon = \varepsilon_0[1 + f_0 \cos(2\omega_{\text{LC,MF}}t)]$. A successful entrainment is marked by $|\alpha|^2$ oscillating at $\omega_{\text{LC,MF}}$, thereby breaking the discrete time translation symmetry imposed by the periodic drive. This constitutes a phase transition from continuous to discrete time crystals [11].

In Fig. 8, we present the response frequencies for 100 trajectories for different driving strengths f_0 . The mean value of the response frequency ω_{peak} is indicated as a circle and its standard deviation is represented by the error bar. The dashed lines refer to the LC frequency according to MF, $\omega_{\text{LC,MF}}$. We observe in Fig. 8(a) that deviations in the response frequencies for all f_0 is present. Hence, the entrainment in a 1D system is not as robust as the one observed in Ref. [11]. The

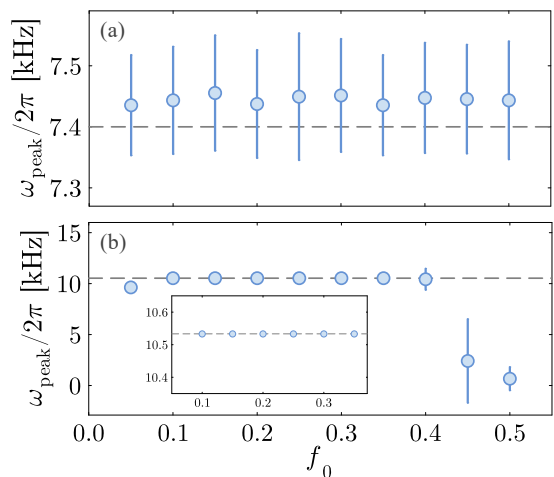


FIG. 8. Response frequencies as a function of the driving strength f_0 for (a) the 1D system with $\omega_{\text{LC,MF}} = 2\pi \times 7.4$ kHz, $\varepsilon_0 = 0.28$, and $\delta_{\text{eff}} = -2\pi \times 7$ kHz, and (b) the 2D system with $\omega_{\text{LC,MF}} = 2\pi \times 10.533$ kHz, $\varepsilon_0 = 0.7375$, and $\delta_{\text{eff}} = -2\pi \times 7.4$ kHz. The driving frequency is $\omega_{\text{dr}} = 2\omega_{\text{LC,MF}}$. The error bars denote the standard deviation of the response frequencies obtained for 100 trajectories within TWA.

weak entrainment can be attributed to the strong shot-to-shot variations of the LC frequency in 1D as discussed in the previous subsection. While $\omega_{\text{LC,MF}}$ is fluctuating for each trajectory, the driving frequency is fixed to just one value for all those trajectories. That is, not all trajectories are resonantly driven, leading to deviations of the response frequency even for smaller values of f_0 in 1D. In contrast, the 2D case exhibits a more robust entrainment with zero standard deviation for $f_0 \in [0.1, 0.35]$. This demonstrates that, while a 2D system also experiences shot-to-shot fluctuations of the LC frequency (see Fig. 7(b)), albeit less likely and weaker than the 1D case, it can still result to a successful entrainment as seen in Fig. 8(b). This is further corroborated by a comparison of the 1D case in Fig. 8(a) and the zoomed-in view of the results for 2D in the inset of Fig. 8(b), wherein the standard deviations are considerably higher in 1D than in 2D.

V. CONCLUSIONS

In summary, we have explored the role of quantum noise in the emergence and entrainment of LCs in an atom-cavity system. Specifically, we compare the photon dynamics obtained using MF and TWA in the 1D and 2D regimes. The TWA allows us to freely switch on and off the stochastic noise in time associated with the cavity dissipation. We found that the inclusion of stochastic noise results to an earlier onset of LCs for smaller pump intensities or, equivalently, light-matter interaction strengths, compared to the corresponding mean-field prediction. In particular, stochastic noise suppresses the high-frequency oscillations in the SR phase, which in turn reveals an earlier signal for the onset of LCs through weak yet detectable oscillations at the expected LC frequency. Furthermore, we have demonstrated that the shot-to-shot fluctuations

of the LC frequency are larger in the 1D limit compared to the 2D limit of the atom-cavity system. This then results to less robust entrainment in 1D as some of the trajectories oscillate at frequencies that are non-resonant with respect to the applied periodic drive of the pump intensity.

Our work highlights the unique role that quantum noise plays in the emergence and stability of dynamical phases, such as limit cycles and time crystals. In particular, we have shown that the fluctuations corresponding to the photon dissipation, a necessary ingredient for beyond mean-field approaches in open quantum systems to ensure that the bosonic commutation relations for the photons are preserved, may reveal a temporal order, or some hints of it, that is otherwise hidden or completely absent in a standard mean-field theory. Resonance phenomena involving dynamical phases, exemplified in this work by entrainment of LCs, can be adversely af-

ected by quantum fluctuations of the initial state depending on the rigidity of the characteristic frequency of the dynamical phase. It would be interesting to explore in future works these phenomena in the full quantum regime, which may aid in the quest for understanding the quantum origins of various behaviours in nonlinear dynamics, such as the appearance of LCs and bifurcations of stable states [17].

ACKNOWLEDGEMENTS

R.J.L.T. and J.G.C. acknowledge support from the DOST-ASTI's COARE high-performance computing facility. This work was funded by the UP System Balik PhD Program (OVPAAB-PhD-2021-04).

-
- [1] K. Matsumoto and I. Tsuda, Noise-induced order, *Journal of Statistical Physics* **31**, 87 (1983).
- [2] C. Zhou and J. Kurths, Noise-Induced Phase Synchronization and Synchronization Transitions in Chaotic Oscillators, *Physical Review Letters* **88**, 230602 (2002).
- [3] Z. G. Nicolaou, M. Sebek, I. Z. Kiss, and A. E. Motter, Coherent Dynamics Enhanced by Uncorrelated Noise, *Physical Review Letters* **125**, 094101 (2020).
- [4] L. J. I. Moon, P. M. Schindler, Y. Sun, E. Druga, J. Knolle, R. Moessner, H. Zhao, M. Bukov, and A. Ajoy, *Experimental observation of a time rondeau crystal: Temporal Disorder in Spatiotemporal Order* (2024), arXiv:2404.05620 [quant-ph].
- [5] H. Zhao, J. Knolle, and R. Moessner, Temporal disorder in spatiotemporal order, *Phys. Rev. B* **108**, L100203 (2023).
- [6] P. Kongkhambut, J. Skulte, L. Mathey, J. G. Cosme, A. Hemmerich, and H. Keßler, Observation of a continuous time crystal, *Science* **377**, 670 (2022).
- [7] T. L. Heugel, A. Eichler, R. Chitra, and O. Zilberberg, The role of fluctuations in quantum and classical time crystals, *SciPost Phys. Core* **6**, 053 (2023).
- [8] F. Piazza and H. Ritsch, Self-Ordered Limit Cycles, Chaos, and Phase Slippage with a Superfluid inside an Optical Resonator, *Phys. Rev. Lett.* **115**, 163601 (2015).
- [9] H. Keßler, J. G. Cosme, M. Hemmerling, L. Mathey, and A. Hemmerich, Emergent limit cycles and time crystal dynamics in an atom-cavity system, *Phys. Rev. A* **99**, 053605 (2019).
- [10] H. Keßler, J. G. Cosme, C. Georges, L. Mathey, and A. Hemmerich, From a continuous to a discrete time crystal in a dissipative atom-cavity system, *New J. Phys.* **22**, 085002 (2020).
- [11] P. Kongkhambut, J. G. Cosme, J. Skulte, M. A. M. Armijos, L. Mathey, A. Hemmerich, and H. Keßler, Observation of a phase transition from a continuous to a discrete time crystal, *Reports on Progress in Physics* **87**, 080502 (2024).
- [12] M. Krishna, P. Solanki, M. Hajdušek, and S. Vinjanampathy, Measurement-Induced Continuous Time Crystals, *Phys. Rev. Lett.* **130**, 150401 (2023).
- [13] A. Greilich, N. E. Kopteva, A. N. Kamenskii, P. S. Sokolov, V. L. Korenev, and M. Bayer, Robust continuous time crystal in an electron–nuclear spin system, *Nature Physics* **20**, 631 (2024).
- [14] I. Carraro-Haddad, D. L. Chafatinos, A. S. Kuznetsov, I. A. Papuccio-Fernández, A. A. Reynoso, A. Bruchhausen, K. Biermann, P. V. Santos, G. Usaj, and A. Fainstein, Solid-state continuous time crystal in a polariton condensate with a built-in mechanical clock, *Science* **384**, 995 (2024).
- [15] H. Ritsch, P. Domokos, F. Brennecke, and T. Esslinger, Cold atoms in cavity-generated dynamical optical potentials, *Rev. Mod. Phys.* **85**, 553 (2013).
- [16] T. D. Farokh Mivehvar, Francesco Piazza and H. Ritsch, Cavity QED with quantum gases: new paradigms in many-body physics, *Advances in Physics* **70**, 1 (2021).
- [17] S. Dutta, S. Zhang, and M. Haque, *On the quantum origin of limit cycles, fixed points, and critical slowing down* (2024), arXiv:2405.08866 [quant-ph].
- [18] A. Polkovnikov, Phase space representation of quantum dynamics, *Ann. Phys.* **325**, 1790 (2010).
- [19] J. G. Cosme, C. Georges, A. Hemmerich, and L. Mathey, Dynamical Control of Order in a Cavity-BEC System, *Phys. Rev. Lett.* **121**, 153001 (2018).
- [20] R. J. L. Tuquero, J. Skulte, L. Mathey, and J. G. Cosme, Dissipative time crystal in an atom-cavity system: Influence of trap and competing interactions, *Phys. Rev. A* **105**, 043311 (2022).
- [21] J. G. Cosme, J. Skulte, and L. Mathey, Time crystals in a shaken atom-cavity system, *Phys. Rev. A* **100**, 053615 (2019).
- [22] H. Keßler, P. Kongkhambut, C. Georges, L. Mathey, J. G. Cosme, and A. Hemmerich, Observation of a Dissipative Time Crystal, *Phys. Rev. Lett.* **127**, 043602 (2021).
- [23] I. Carusotto and C. Ciuti, Quantum fluids of light, *Rev. Mod. Phys.* **85**, 299 (2013).
- [24] P. B. Blakie, A. S. Bradley, M. J. Davis, R. J. Ballagh, and C. W. Gardiner, Dynamics and statistical mechanics of ultracold Bose gases using c-field techniques, *Adv. Phys.* **57**, 363 (2008).
- [25] K. Baumann, C. Guerlin, F. Brennecke, and T. Esslinger, Dicke quantum phase transition with a superfluid gas in an optical cavity, *Nature* **464**, 1301 (2010).
- [26] D. Nagy, G. Szirmai, and P. Domokos, Self-organization of a Bose-Einstein condensate in an optical cavity, *Eur. Phys. J. D* **48**, 127 (2008).
- [27] J. Klinder, H. Keßler, M. Wolke, L. Mathey, and A. Hemmerich, Dynamical phase transition in the open Dicke model, *Proc. Natl. Acad. Sci. USA* **112**, 3290 (2015).
- [28] P. Gao, Z.-W. Zhou, G.-C. Guo, and X.-W. Luo, Self-organized limit cycles in red-detuned atom-cavity systems, *Phys. Rev. A*

- [107, 023311 \(2023\)](#).
- [29] J. G. Cosme, J. Skulte, and L. Mathey, Bridging closed and dissipative discrete time crystals in spin systems with infinite-range interactions, [Phys. Rev. B **108**, 024302 \(2023\)](#).
- [30] S. H. Strogatz, *Nonlinear Dynamics and Chaos: With Applications to Physics, Biology, Chemistry, and Engineering, in Studies in Nonlinearity* (Westview, Cambridge, 2000).
- [31] M. H. Jensen, P. Bak, and T. Bohr, Complete Devil's Staircase, Fractal Dimension, and Universality of Mode-Locking Structure in the Circle Map, [Phys. Rev. Lett. **50**, 1637 \(1983\)](#).
- [32] M. H. Jensen, P. Bak, and T. Bohr, Transition to chaos by interaction of resonances in dissipative systems. I. Circle maps, [Phys. Rev. A **30**, 1960 \(1984\)](#).